Tohoku J. Exp. Med., 2022, **256**, 151-160

Application of Diffusion Tensor Imaging Fiber Tractography for Human Masseter Muscle

Takehiko Sugano,[1] Nobuhiro Yoda,[1] Toru Ogawa,[1] Teruo Hashimoto,[2] Kenta Shobara,[1] Kuniyasu Niizuma,[3,4,5] Ryuta Kawashima[2] and Keiichi Sasaki[1]

[1]Division of Advanced Prosthetic Dentistry, Tohoku University Graduate School of Dentistry, Sendai, Miyagi, Japan
[2]Institute of Development, Aging and Cancer, Tohoku University, Sendai, Miyagi, Japan
[3]Department of Neurosurgical Engineering and Translational Neuroscience, Graduate School of Biomedical Engineering, Tohoku University, Sendai, Miyagi, Japan
[4]Department of Neurosurgical Engineering and Translational Neuroscience, Tohoku University Graduate School of Medicine, Sendai, Miyagi, Japan
[5]Department of Neurosurgery, Tohoku University Graduate School of Medicine, Sendai, Miyagi, Japan

Diffusion tensor imaging (DTI) has been used to indicate the direction of nerve and muscle fibers by using the characteristics that water molecules preferentially diffuse along the fibrous structure. However, DTI fiber tractography for multipennate muscles, such as the masseter muscle, is challenging due to a lack of data regarding the imaging parameters. This study aimed to determine the optimal DTI parameters for masseter muscle fiber tractography. A 27-year-old healthy man voluntarily underwent DTI and T1-weighted magnetic resonance imaging of the right masseter muscle. Four imaging parameter settings were created by combining the following parameters that particularly affect the signal-to-noise ratio: b-value, number of excitations (NEX), and number of motion probing gradient (MPG) directions. DTI fiber tractography was performed using specific software for each parameter setting. The length and orientation of the muscle fibers in each layer were calculated. As a result, the masseter muscle fibers of each layer were identified on DTI. Although the detected fiber length was affected significantly by the imaging parameters, the fiber orientation was insignificantly affected. The appropriate combination of the b-value, NEX, and the number of MPG directions for masseter muscle fiber tractography could be determined based on previously reported anatomical data of the masseter muscle fibers. DTI may enable the non-invasive evaluation of masseter muscle fiber length and orientation. Elucidation of the details of masseter muscle fiber orientation is useful in evaluating stomatognathic biomechanics and muscle disorders.

Keywords: biomechanics; diffusion tensor imaging; fiber tractography; magnetic resonance imaging; masseter muscle
Tohoku J. Exp. Med., 2022 February, **256** (2), 151-160.

Introduction

The masseter muscle has a complex internal multipennate structure enabling highly functional differentiation (Ogawa et al. 2006; Curtis et al. 2012). Gaudy et al. (2000) found that the human masseter muscle has three layers, with each layer composed of multiple muscle bundles arranged in various directions. Another anatomical study reported that the superficial head of the masseter muscle has an average of three layers with five aponeuroses, while the deep head has two layers with two aponeuroses (Ebrahimi 2015). Furthermore, the internal architecture of the masseter muscle reportedly varies markedly between individuals with respect to the number, shape, and location of the compartments delineated by aponeuroses (Cioffi et al. 2012).

Many studies have demonstrated the properties of local activity inside the masseter muscle by performing electromyography using needle or wire electrodes (Tonndorf et al. 1989; van Dijk et al. 2016; Malik et al. 2018). In addition, ultrasonographic observations have revealed significant differences in mean fiber bundle length

Received August 29, 2021; revised and accepted November 3, 2021. Published online February 26, 2022; doi: 10.1620/tjem.256.151.
Correspondence: Nobuhiro Yoda, Division of Advanced Prosthetic Dentistry, Tohoku University Graduate School of Dentistry, 4-1 Seiryo-machi, Aoba-ku, Sendai, Miyagi 980-8575, Japan.
e-mail: nobuhiro.yoda.e2@tohoku.ac.jp

between the relaxed and contracted states only in the superficial layer of the superficial head (Gheorghe et al. 2021), suggesting that masseter muscle contraction varies among layers. Furthermore, muscle functional magnetic resonance imaging (MRI) has revealed that the position of the occlusal point during unilateral single tooth clenching significantly affects the activity inside the masseter muscle (Okada et al. 2016).

The masseter muscle is the most common site of pain in patients with temporomandibular disorders (TMD) (Herpich et al. 2018). Since the location and intensity of masseter muscle pain differs between patients, the international diagnostic criteria for TMD recommends the assessment of nine palpation points in one muscle to examine pain severity (Ohrbach 2014). It is thus important to elucidate the details of its pathophysiology. Variation in the pain site probably reflects the individual function and morphology in the maxillofacial region (Pereira et al. 2007; Curtis et al. 2012). Above-mentioned functional differentiation inside the masseter muscle can also affect variation in the pain site. However, it is difficult to investigate the relationship between muscle function and pain site in patients with TMD, because previous methods, such as electromyographic techniques, are somewhat invasive and complex in regard to clinical examinations. Therefore, it remains unclear how the complex masseter muscle structure is associated with site differentiation of muscle pain in TMD. Medical image analyses, such as computed tomography and MRI, are useful for static morphological assessment of muscles (Ng et al. 2009; Chen et al. 2020). Although these image analyses can detect abnormal states in muscles and other hard and soft tissues, it is difficult to comprehend internal muscle structural changes while being used. Ultrasonography can also show the internal morphological structure of the muscle fiber bundle orientation and pennate angle on the surface of skeletal muscle (Kawakami et al. 1993; Kubo et al. 2006; Cronin and Lichtwark 2013). However, as the ultrasound signal is attenuated with depth in the muscle, it is difficult to examine the fiber condition in deeper areas within the masseter muscle.

Diffusion-weighted imaging (DWI), which is a type of MRI, demonstrates the irregular diffusion motion of water molecules as seen in Brownian motion (Sotak 2004). Diffusion tensor imaging (DTI), which is based on DWI, can detect the changes in MRI signals due to self-diffusion of water molecules. DTI has mainly been used to identify cranial nerves for both clinical and research purposes. Recently, DTI has been used for analysis of skeletal muscle fiber orientation. Some studies have reported that DTI fiber tractography can be used as a non-invasive method of visualizing muscle fiber orientation and internal structural changes (Oudeman et al. 2016; Charles et al. 2018). However, the application of DTI fiber tractography in the masseter muscle, a multipennate muscle, is challenging because insufficient information is available to determine the basic imaging parameters. The purpose of this study was to determine the optimal DTI parameters for masseter muscle fiber tractography and to establish a method for evaluating muscle fiber orientation in the masseter muscle.

Materials and Methods

Participant

All procedures were performed in accordance with the Declaration of Helsinki and Ethical Guidelines for Medical and Health Research Involving Human Subjects issued by the Japanese Ministry of Health, Labour and Welfare. This study protocol was approved by the research ethics committee of Tohoku University Graduate School of Dentistry (reference number: 2019-3-017) and was registered in the UMIN database (registration number 000080691). The participant provided written informed consent after the study protocol was fully explained. The right masseter muscle of this healthy 27-year-old man was studied.

MRI image acquisition

A 3.0T MRI system (Achieva 3.0T Quasar Dual, Philips, Amsterdam, Netherlands) was used for MRI. The participant was in the supine position with his head fixed at a 90° angle so that his eyes faced the ceiling and therefore the Frankfurt horizontal (FH) plane was perpendicular to the ground during scanning. The mandibular rest position was previously recorded with dental occlusal materials (Correct Quick Bite, Pentron Japan Inc., Tokyo, Japan) and the recorded material was placed between the upper and lower dentitions to maintain the mandibular position during the MRI scan. The participant was instructed to relax his entire masticatory muscles as much as possible.

Based on previous reports for DTI tractography of the cranial nerve and skeletal muscle fiber (Mukherjee et al. 2008; Oudeman et al. 2016), the signal-to-noise ratio (SNR) was used as an indicator to investigate the optimal DTI parameters for the masseter muscle fiber tractography. The SNR is particularly affected by the number of motion probing gradient (MPG) directions (Yamamoto et al. 2007), b-value (Steidle and Schick 2006), and number of excitations (NEX) (Johnson et al. 2014). Therefore, the present study focused on these three parameters.

A pair of MPGs is generally applied at regular intervals in DWI. DWI captures the motion of molecules in the direction of the gradient magnetic field by applying a pair of MPGs of the same size and opposite directions at regular time intervals during imaging (Stejskal and Tanner 1965). Jones (2004) reported that at least 30 directions are required to obtain a highly accurate tensor direction and fractional anisotropy (FA) value, while Lee et al. (2006) reported that the results did not differ in the DTI of the cervical cord between 15 and 32 directions. Based on these previous findings, 15 and 32 MPG directions were set as the experimental parameters in this study.

The b-value, which represents the strength of the MPG, is another important parameter in DWI (Froeling et al. 2013). As the b-value increases, the amount of the diffu-

sion-weighting increases and the angular resolution and the fiber extraction ability are improved, but the SNR decreases. The b-value is generally set at 1,000 s/mm^2 for imaging the cranial nerves (Mukherjee et al. 2008). For muscle fiber analysis, studies have suggested that a b-value of 400 to 500 s/mm^2 is suitable for skeletal muscle imaging (Froeling et al. 2013), and that a b-value of 625 s/mm^2 is appropriate for muscle imaging with a 1.5T MRI device (Saupe et al. 2009). Based on these previous reports, b-values of 500 and 700 s/mm^2 were chosen as the experimental values in this study.

As the signal intensity is limited by one scanning, the SNR can be improved by √n times by multiplying the number of NEX. However, the increased scanning time might be an excessive burden for the patient and also lead to motion artifact (Johnson et al. 2014). Therefore, the NEX was set as 1 and 2 in this study.

In consideration of the burden on the participant, a total of four experimental imaging parameter settings with different parameter combinations were used (Table 1). Other parameter settings are shown in Table 2. As a voxel volume of 20 to 30 mm^3 is recommended to ensure sufficient SNR in the DTI of muscle (Oudeman et al. 2016), the voxel size of DTI was set at 27 mm^3.

T1 turbo field echo (T1-TFE) imaging was also used to obtain a reference anatomical image. A total of five scans including four imaging parameter settings for DTI and T1-TFE imaging were performed using the same field of view, which included the entire right masseter muscle and the FH plane as a reference plane. There was a 10-second interval between each imaging scan.

MRI data processing

DICOM (Digital Imaging and Communications in Medicine) data were obtained from the scans and converted to the NIFTI (Neuroimaging Informatics Technology Initiative) format using the free software dcm2nii (Neuropsychology Lab, Columbia, SC, USA) (Li et al. 2016). By analyzing the NIFTI data with the FMRIB Software Library (FSL) diffusion tool (Smith et al. 2004), muscle fiber orientation was obtained. Two free software packages, FSL v6.0 (https://fsl.fmrib.ox.ac.uk/fsl/fslwiki) and MRtrix3 (Tournier et al. 2019), were used for the DTI muscle fiber tractography. The DWI was first resampled to match the T1-TFE voxel size in the FSL. Then, the right masseter muscle was segmented into three layers (superficial, intermediate, and deep), with reference to the T1-TFE images (Fig. 1). The aponeurosis separating each layer confirmed on the images was used as reference for segmentation. This segmentation was performed manually by three experienced dentists and the threshold selection for segmentation was made by joint decisions. The average FA

Table 1. Experimental parameter settings.

Parameter setting abbreviation	500-1-15	500-1-32	500-2-15	700-2-15	T1-TFE
Maximum b-value	500	500	500	700	-
NEX	1	1	2	2	1
MPG direction	15	32	15	15	-
Total scan duration	02:38	05:11	04:23	04:23	05:47

The upper row lists the parameter setting abbreviations; the four combinations of DTI parameters and the T1-weighted MRI parameters are listed. The numbers in the setting abbreviations indicate the b-value, number of excitations (NEX), and number of motion probing gradient (MPG) directions, respectively.
T1-TFE, T1 turbo field echo.

Table 2. Other parameter settings.

	DTI	T1-TFE
Scan technique	Spin echo	Fast field echo
Fast Imaging mode	Echo planar imaging	Turbo field echo
Shot interval (ms)	-	2,000
Flip angle (degrees)	90	8
Field of view (mm)	192	192
Matrix	64 × 64	240 × 240
Imaging option	Sensitivity Encoding	Sensitivity Encoding
Echo time	55	Shortest
Repetition time	3,500	Shortest
Slice thickness (mm)	3	0.80
Voxel size (mm)	3.0 × 3.0 × 3.0	0.8 × 0.8 × 0.8

The above parameters were used for all DTI scans.
DTI, diffusion tensor imaging; T1-TFE, T1 turbo field echo.

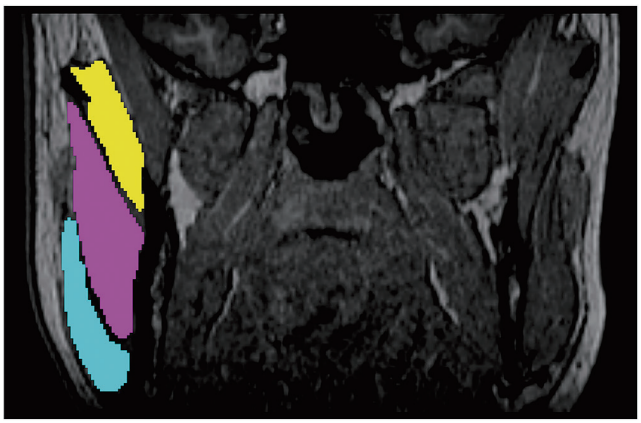

Fig. 1. An example of a layer created on the right masseter muscle (frontal view).
Light blue: superficial layer, magenta: intermediate layer, yellow: deep layer.

value for each layer was also calculated using MRtrix3 software.

Masseter muscle fiber tractography was performed following the procedure of skeletal muscle fiber tractography (Oudeman et al. 2016). The standard setting of MRtrix3 for the fiber tracking algorithm, the Second-order Integration over Fiber Orientation Distributions (Tournier et al. 2010), was employed. The step size was set as 1/2 of the voxel size, and tracking was performed until the FA value became less than 0.02 or the angle change between steps exceeded 30 degrees. In addition, fibers that were shorter than 10 mm were excluded, and a total of 200 fibers were drawn in each layer as pre-processing for the proper tractography with clear visibility and analyzability based on our preliminary experiment. In nerve tractography, the region of interest (ROI) should be set at the origin and end of the nerve fascicle so that only the nerve bundles passing through the ROIs are extracted. However, in the case of masseter muscle fibers, it is difficult to set the ROI for each fiber because of the complex pathway of the specific fibers. Therefore, all voxels in each layer were included as ROIs, and fiber tractography was performed inside the layer. A dedicated program (Convert.exe, Nihon Visual Science Inc., Tokyo, Japan) (http://www.nvs.co.jp/) was used for the extracted fiber analysis. An aggregate of line segments (polyline) was generated by connecting the fibers obtained at each step size. As the polylines can be assumed to be actual masseter muscle fibers, each polyline was referred to as a DTI fiber in this study (Fig. 2).

The three-dimensional (3D) coordinates from DTI fibers were converted to voxel-based labeling information. They fuse with original MRI images, and each DTI fiber was visualized as colored volume data using dedicated software (ExFact VR, Nihon Visual Science Inc., Tokyo,

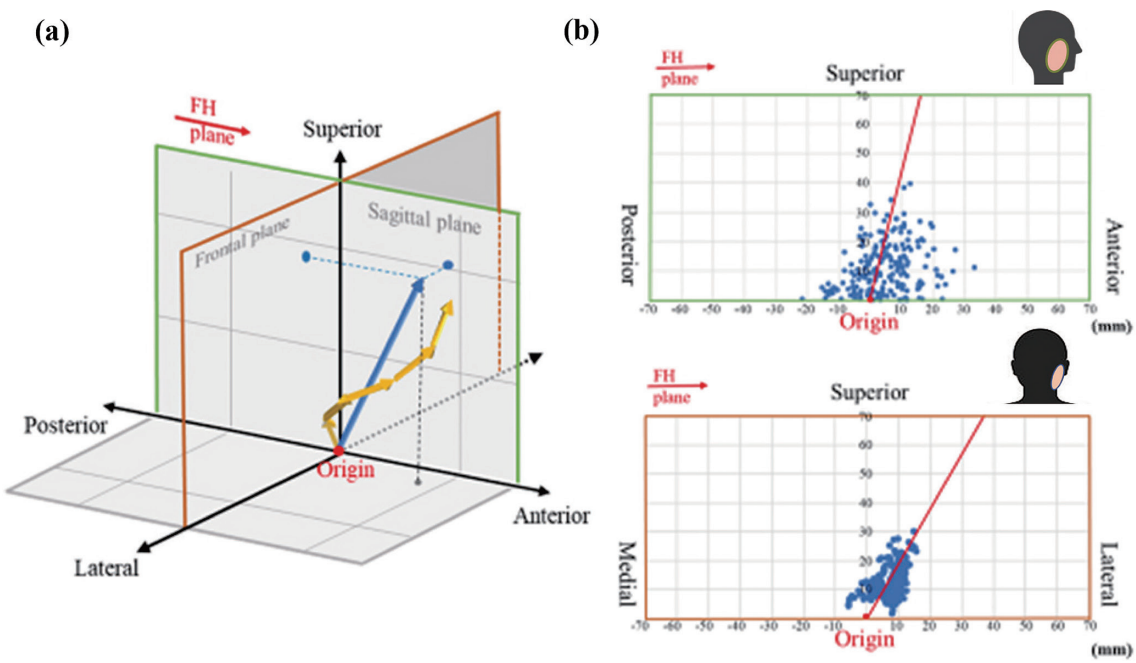

Fig. 2. Diffusion tensor imaging fiber direction analysis.
(a) The fiber direction is determined by the direction of water molecular diffusion for each voxel. Line segments based on the diffusion direction of each voxel are drawn at 1/2 voxel size intervals (orange arrows). By connecting these line segments, fiber tractography follows the fiber structure (DTI fiber). Each DTI fiber is composed of the multiple line segments (polyline), and the 3D orientation of each DTI fiber is simplified as the composite vector of all the line segments (blue arrow). The endpoints of each composite vector are projected in the sagittal and frontal planes (blue dots). (b) An example of DTI fiber projection in the sagittal plane (green fence line) and frontal plane (brown fence line) using the coordinates with reference to the FH plane. The origin of each DTI fiber is unified. The endpoints of 200 composite vectors are plotted as blue dots. The red line shows the average direction of all DTI fibers.
DTI, diffusion tensor imaging; 3D, 3-dimensional.

Japan). Then, the length and direction of each DTI fiber were calculated. The length of the DTI fiber was represented by the sum of the polyline segments. The vectors of all the line segments were synthesized to obtain the direction of the DTI fiber. The compositions of vectors were projected on the sagittal plane of the participant, and the average DTI fiber direction of each layer was calculated. The individual DTI fiber structures were visualized by a software product (ExFact Analysis for Fiber, Japan Visual Science Co., Ltd., Tokyo, Japan).

Statistical analysis

Two-way analysis of variance (ANOVA) was performed to evaluate the effects of muscle layer and DTI parameter setting on DTI fiber length and direction, followed by a post hoc Tukey test. A p value of less than 0.05 was considered statistically significant. The statistical analyses were carried out using SPSS version 26 (IBM, NY, USA).

Results

FA value

The average FA value of each masseter muscle layer under each imaging parameter setting is shown in Table 3. In each column, the average FA value of superficial and intermediate layers tended to be larger than that of the deep layer.

DTI fiber tractography

Fig. 3 shows the DTI fiber tractography results. There are some differences in the DTI fiber representation depending on the imaging parameters. However, the common feature under all parameter settings was that the fiber orientation differed between the muscle layers and was

Table 3. Fractional anisotropy (FA) value under each imaging parameter setting.

		Parameter setting			
		500-1-15	500-1-32	500-2-15	700-2-15
Muscle layer	Superficial	0.43	0.36	0.39	0.33
	Intermediate	0.48	0.32	0.32	0.32
	Deep	0.28	0.26	0.25	0.23

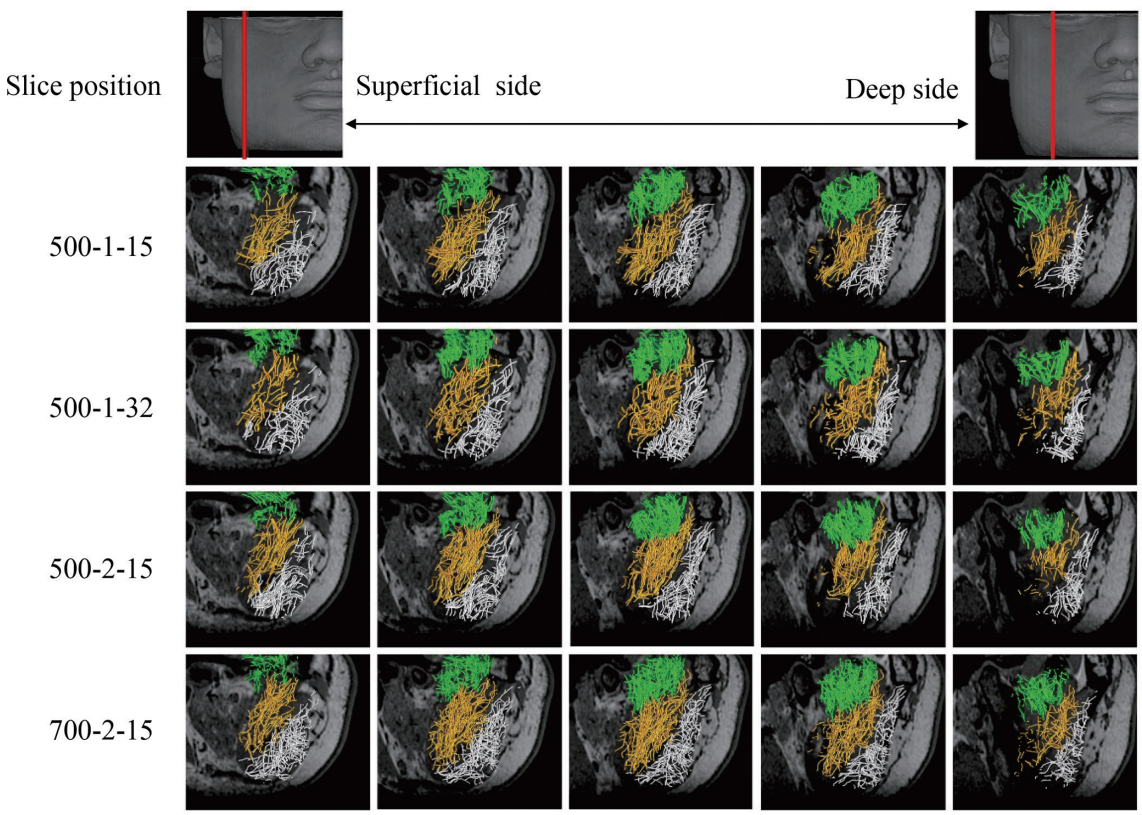

Fig. 3. Schema of diffusion tensor imaging fibers (displayed in the sagittal plane).
Diffusion tensor imaging (DTI) fibers are drawn on the T1-TFE images. The displayed sagittal view is five slices every 4 voxels (3.2 mm) from the superficial side to the deep side, and the sagittal plane is viewed from the right side. Superficial layer, white; intermediate layer, yellow; deep layer, green.

heterogeneous within each muscle layer.

Table 4 shows the average DTI fiber length in each masseter muscle layer under each DTI parameter setting. The DTI fiber length was significantly influenced by the muscle layer (Table 4) and parameter setting (Table 4). The average fiber length was significantly shorter in the deep muscle layer than in the superficial and intermediate layers, but did not significantly differ between the superficial and intermediate layers. Except for the lack of difference in average fiber length between the 500-1-15 and 500-2-15 DTI parameter settings, significant differences were found between all other pairs of settings.

Fig. 4 shows schemas expressing the distribution of direction and length of the DTI fibers in the sagittal plane. The average fiber direction was anterior-superior in the superficial and intermediate layers, and posterior-superior in the deep layer. The fiber direction was significantly influenced by the muscle layer ($P < 0.01$, ANOVA). The

Table 4. Average diffusion tensor imaging (DTI) fiber length (mm) under each parameter setting.

		Parameter setting				
		500-1-15	500-1-32	500-2-15	700-2-15	
Muscle layer	Superficial	21.2 ± 8.9	18.4 ± 7.9	20.6 ± 9.6	23.8 ± 11.8	ANOVA for muscle layers ($P < 0.01$) Tukey HSD test Superficial vs. Intermediate (Not Significant) Deep < Superficial ($P < 0.01$), Intermediate ($P < 0.01$)
	Intermediate	20.1 ± 9.7	16.6 ± 5.9	21.1 ± 9.3	26.2 ± 14.1	
	Deep	16.5 ± 5.7	15.8 ± 5.3	18.5 ± 7.7	20.1 ± 7.6	
		ANOVA for parameter settings ($P < 0.001$) Tukey HSD test 500-1-15 > 500-1-32 ($P < 0.01$) 500-1-15 vs. 500-2-15 (Not Significant) 500-1-15 < 700-2-15 ($P < 0.01$) 500-1-32 < 500-2-15 ($P < 0.01$) 500-1-32 < 700-2-15 ($P < 0.01$) 500-2-15 < 700-2-15 ($P < 0.01$)				

Data are presented as mean ± standard deviation.
The results of the two-way ANOVA and post hoc Tukey test are also shown in the Table.

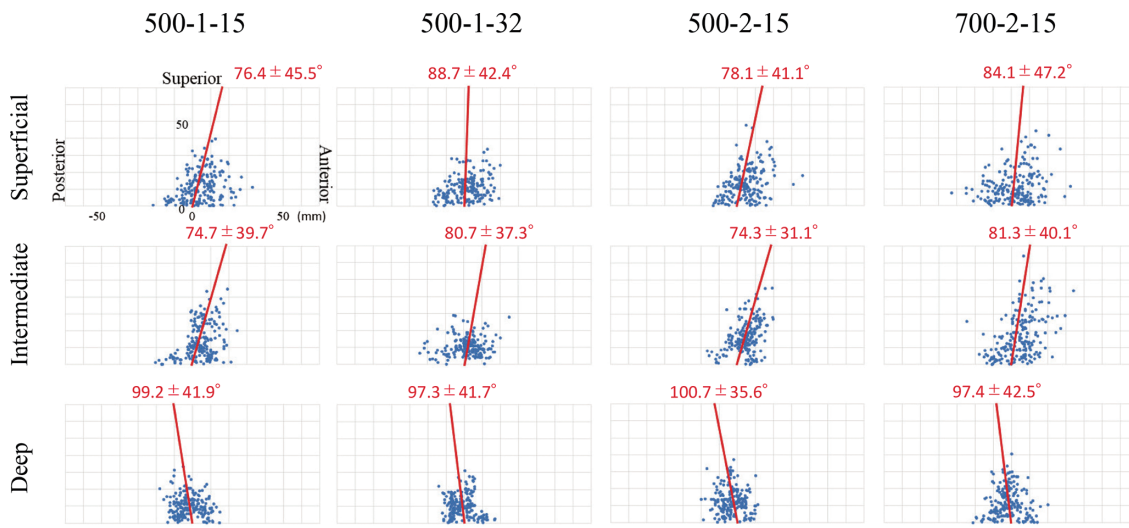

Statistical significance		
Two-way ANOVA	Three layers; $P < 0.01$	Four parameter settings; Not Significant
Tukey test for layers	Deep > Superficial ($P < 0.01$), Intermediate ($P < 0.01$) Superficial vs. Intermediate (Not Significant)	

Fig. 4. Distribution of the length and direction of the diffusion tensor imaging fibers in the sagittal plane.
View of the sagittal plane from the right side. Red-colored values represent the mean fiber direction and standard deviation. There are significant differences between the three muscle layers (superficial, intermediate, and deep). There are no significant differences among the parameter settings (500-1-15, 500-1-32, 500-2-15, and 700-2-15).

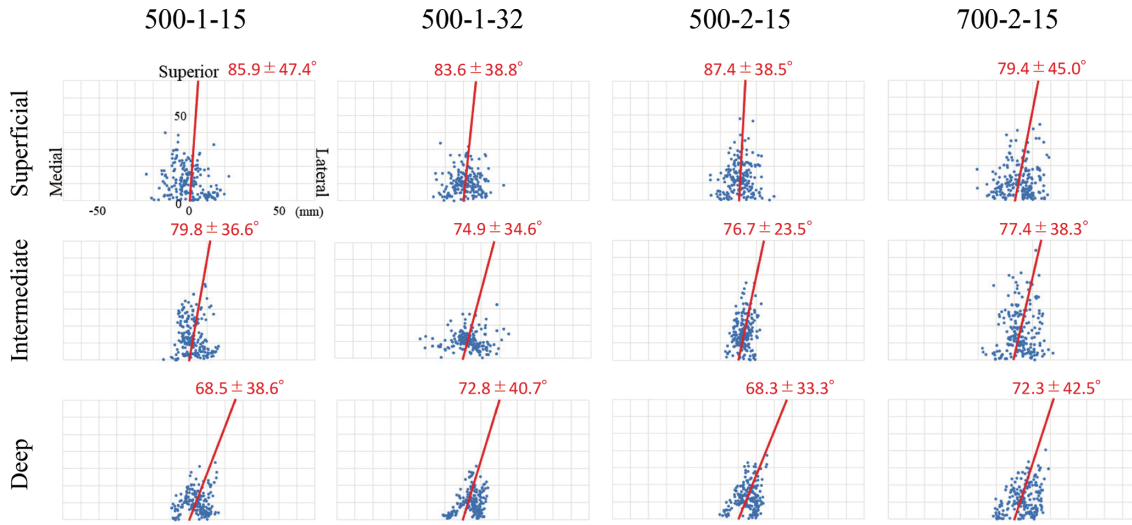

Statistical significance		
Two-way ANOVA	Three layers; $P < 0.01$	Four parameter settings; Not Significant
Tukey HSD test for layers	Superficial > Intermediate ($P < 0.01$)	
	Intermediate > Deep ($P < 0.01$)	
	Superficial > Deep ($P < 0.01$)	

Fig. 5. Distribution of the length and direction of the diffusion tensor imaging fibers in the frontal plane. View of the frontal plane from the posterior aspect. Red-colored values represent the mean fiber direction and standard deviation. There are significant differences between the three muscle layers (superficial, intermediate, and deep). There are no significant differences among the parameter settings (500-1-15, 500-1-32, 500-2-15, and 700-2-15).

fiber direction in the deep layer was significantly different to that in the superficial and intermediate layers ($P < 0.01$, Tukey test), but did not significantly differ between the superficial and intermediate layers.

Fig. 5 shows schemas expressing the distribution of direction and length of the DTI fibers in the frontal plane. The fiber direction was significantly influenced by the muscle layer ($P < 0.01$, ANOVA); significant differences were detected between all three layers [superficial > intermediate ($P < 0.01$), intermediate > deep ($P < 0.01$), superficial > deep ($P < 0.01$, Tukey test)]. This shows that the fibers in the superficial layer were closest to craniocaudal direction, those in the deep layer were most tilted, and those in the intermediate layer were in between these two orientations.

Discussion

To establish a method for evaluating the muscle fiber orientation in the masseter muscle, this study was preliminarily conducted voluntarily on a healthy man. Shiraishi et al. (2012) performed DTI of the masseter muscle and demonstrated that the average FA value was 0.31 for the superficial layer and 0.29 for the intermediate layer. Although the device they used was a 1.5T-scanner, which was a different device than used in this study, the FA values in this experiment were generally similar to their results. The appropriate DTI parameters for masseter muscle fiber tractography have been unclear. To the best of our knowledge, this study is the first attempt to examine the appropriate parameters of DTI tractography for the human masseter muscle, which has a complex multipennate internal structure.

The pennation angle of the masseter muscle is defined as the angle formed between the aponeurosis and muscle fibers, which is difficult to measure accurately on MRI. Therefore, it is necessary to confirm whether DTI can be used to assess the complicated fiber structure in the masseter muscle. Although previous research has used DTI to calculate the pennation angle in infants (Falcinelli et al. 2018), it is difficult to perform a similar analysis of live adult masseter muscles with a more complex structure. Therefore, in the present study, the masseter muscle was divided into three layers, and the validity of DTI parameters was verified from the viewpoint of the fiber direction and length in each layer, although only on a qualitative basis. This enabled the optimal imaging parameters to be verified as an essential step for further detailed analysis of the structure of the pennate masseter muscle. In addition, the present study used 3D coordinates in the FH and sagittal planes to analyze DTI fiber direction. The method used in the present study might be useful for normalizing the DTI fiber directions and for future comparison of several participants with different maxillofacial morphologies.

The spin relaxation time of skeletal muscle tissue is about 35 milliseconds, which is shorter than that of nerve fibers. In addition, the water proton density of muscles is generally lower than that of brain tissue (Froeling et al.

2013). Therefore, specific parameter settings, such as the b-value, NEX, and number of MPG directions, are required for DTI muscle fiber tractography (Jones 2004; Froeling et al. 2013). As the restraint scanning time should be minimized to avoid participant fatigue and reduce motion artifact, four imaging parameter settings with combinations of these three parameters were set up.

The fiber length and orientation detected by DTI fiber tractography is difficult to validate in living humans (Voskuilen et al. 2019). The reproducibility of DTI fibers regarding the length and direction of muscle bundles was therefore validated using the results of previous anatomical cadaver analysis. According to the study by van Eijden and Raadsheer (1992), the masseter muscle fiber length ranged from 19.0 to 30.3 mm, and the deep part had an average fiber length that was 5% shorter than the superficial part. Gheorghe et al. (2021) reported that the mean muscle fiber bundle length ranged from 12.1 to 21.1 mm in the relaxed state. In the present study, fiber length was significantly influenced by parameter settings. As it is difficult to verify the validity of the muscle fiber length obtained by DTI in a human study, animal experiments may be necessary to verify the parameters in the future.

The average direction of the DTI fibers in the sagittal plane significantly differed between the superficial/intermediate layers and the deep layer (Fig. 4), which is consistent with the results of previous anatomical studies (Gaudy et al. 2000; Ebrahimi 2015). The average direction of the DTI fibers in the frontal plane significantly differed between all three layers (Fig. 5), and coincided with the directions of the aponeuroses seen in the T1-TFE images. Fiber direction was not significantly influenced by parameter settings.

The average DTI fiber length was different under each imaging parameter setting. A higher b-value might decrease the SNR, and a decreased SNR is considered to have a risk for deviation from the actual muscle fiber length in DTI fiber tractography. This might be the reason for the significantly longer DTI fiber length under the 700-2-15 setting compared with the other parameter settings (Table 4). In addition, the FA value under the 700-2-15 parameter setting was lower than that of those under the other parameter settings (Table 3). As the FA value is affected by the SNR, the FA value under the 700-2-15 parameter setting may be lower due to the low SNR and high b-value. A low SNR may increase the number of inaccurate DTI fibers that deviate from the actual muscle fiber orientation (Froeling et al. 2013). Therefore, inappropriate fiber connection might occur, resulting in the detection of overly long fibers under the 700-2-15 parameter setting.

To determine the optimal b-value for DTI fiber tractography, it is necessary to consider the balance between the sensitivity of molecular diffusion weighting (maximized at high b-values) and the SNR required for accurate fiber tractography (maximized at low b-values). The present results suggest that a b-value of 500 might be appropriate for masseter muscle fiber tractography. Increasing the NEX improves the SNR and reduces measurement errors (Johnson et al. 2014). The effect of the NEX can be evaluated by comparing results between the 500-1-15 and 500-2-15 parameter settings. There was no significant difference in fiber length between the 500-1-15 and 500-2-15 parameter settings (Table 4). However, the DTI fibers were visually more uniform under the 500-2-15 parameter setting than the 500-1-15 parameter setting (Fig. 3) meaning that a NEX of 2 is better than 1. However, increasing the NEX prolongs the scanning time, which increases the risk of motion artifact (Lee et al. 2006). Therefore, it is difficult to use a NEX of 3 or more when performing DTI in humans. The effect of the number of MPG directions can be evaluated by comparing the results obtained under the 500-1-15 parameter setting with those obtained under the 500-1-32 setting. The fiber length was significant longer under the parameter setting of 500-1-15 than 500-1-32 (Table 4). Furthermore, the fiber length under the 500-1-32 parameter setting was shorter than that reported by van Eijden and Raadsheer (1992). Theoretically, a higher number of diffusion gradient directions yields more accurate diffusion tensor information. However, the longer scanning times also carry a greater risk of motion artifact (Lee et al. 2006). In DTI fiber tractography of the masseter muscle, the effect of the number of MPG directions was small; the present results suggest that about 15 directions may be sufficient.

Although the application of DTI showed the fiber tractography of the human masseter muscle, there are still limitations that need to be addressed. The segmentation of the muscle, which affected the fiber tracking algorithm, was performed manually in the present study. However, because the muscle segmentation has a large impact on the results, an alternative automated method is preferable. In addition, although commonly used stop criteria for DTI tractography were applied in the present study, the measurement of muscle architecture by DTI tractography is reportedly sensitive to variations in the stop criteria (Bolsterlee et al. 2019). The impact of the stop criteria requires verification in a future study.

While the usefulness of the DTI fiber tractography was detected in this study, to validate the reproducibility of DTI fiber tractography further animal and/or human studies are necessary. The application of DTI may be useful as a non-invasive method of evaluating human masseter muscle fibers, although some improvements are needed. Elucidation of the detailed orientation of masseter muscle fibers may also be useful in examining the stomatognathic biomechanics considering the muscle fiber dynamics.

In conclusion, DTI is a non-invasive method of clarifying the length and orientation of masseter muscle fibers. The effects of DTI parameters, such as the b-value, NEX, and number of MPG directions on fiber tractography, have been clarified. The appropriate DTI parameters to evaluate the masseter muscle fiber length and orientation are suggested as a b-value of 500, NEX of 2, and the number of MPG directions to be 15.

Acknowledgments

We thank NVS for developing the specific software for conducting the analysis of DTI. We thank Kelly Zammit, BVSc, from Edanz Group (https://jp.edanz.com/ac) for editing a draft of this manuscript. This study was fully supported by grants-in-aid for Scientific Research (C) (20K10066) from the Japan Ministry of Education, Culture, Sports, Science and Technology.

Conflict of Interest

The authors declare no conflict of interest.

References

Bolsterlee, B., D'Souza, A. & Herbert, R.D. (2019) Reliability and robustness of muscle architecture measurements obtained using diffusion tensor imaging with anatomically constrained tractography. *J. Biomech.*, **86**, 71-78.

Charles, J.P., Moon, C.H. & Anderst, W. (2018) Determining subject-specific lower-limb muscle architecture data for musculoskeletal models using diffusion tensor MRI. *J. Biomech. Eng.*, **141**, 060905.

Chen, W., Li, Y., Dyer, B.A., Feng, X., Rao, S., Benedict, S.H., Chen, Q. & Rong, Y. (2020) Deep learning vs. atlas-based models for fast auto-segmentation of the masticatory muscles on head and neck CT images. *Radiat. Oncol.*, **15**, 176.

Cioffi, I., Gallo, L.M., Palla, S., Erni, S. & Farella, M. (2012) Macroscopic analysis of human masseter compartments assessed by magnetic resonance imaging. *Cells Tissues Organs*, **195**, 465-472.

Cronin, N.J. & Lichtwark, G. (2013) The use of ultrasound to study muscle-tendon function in human posture and locomotion. *Gait Posture*, **37**, 305-312.

Curtis, D.A., Gansky, S.A. & Plesh, O. (2012) Deep and superficial masseter muscle blood flow in women. *J. Prosthodont.*, **21**, 472-477.

Ebrahimi, E. A. (2015) Musculo-aponeurotic architecture of the human masseter muscle: a three-dimensional cadaveric study. Master's Thesis, Discipline of Oral and Maxillofacial Surgery, University of Toronto.

Falcinelli, C., Li, Z., Lam, W.W., Stanisz, G.J., Agur, A.M. & Whyne, C.M. (2018) Diffusion-tensor imaging versus digitization in reconstructing the masseter architecture. *J. Biomech. Eng.*, **140**, 111010.

Froeling, M., Nederveen, A.J., Nicolay, K. & Strijkers, G.J. (2013) DTI of human skeletal muscle: the effects of diffusion encoding parameters, signal-to-noise ratio and T2 on tensor indices and fiber tracts. *NMR Biomed.*, **26**, 1339-1352.

Gaudy, J.F., Zouaoui, A., Bravetti, P., Charrier, J.L. & Guettaf, A. (2000) Functional organization of the human masseter muscle. *Surg. Radiol. Anat.*, **22**, 181-190.

Gheorghe, T.I., Leekam, R., Lam, E.W.N., Perschbacher, S., Liebgott, B. & Agur, A.M.R. (2021) A dynamic ultrasonographic in vivo study of the musculoaponeurotic architecture of the human masseter muscle. *Oral Surg. Oral Med. Oral Pathol. Oral Radiol.*, **132**, 609-615.

Herpich, C.M., Gomes, C., Dibai-Filho, A.V., Politti, F., Souza, C.D.S. & Biasotto-Gonzalez, D.A. (2018) Correlation between severity of temporomandibular disorder, pain intensity, and pressure pain threshold. *J. Manipulative Physiol. Ther.*, **41**, 47-51.

Johnson, C.L., Holtrop, J.L., McGarry, M.D., Weaver, J.B., Paulsen, K.D., Georgiadis, J.G. & Sutton, B.P. (2014) 3D multislab, multishot acquisition for fast, whole-brain MR elastography with high signal-to-noise efficiency. *Magn. Reson. Med.*, **71**, 477-485.

Jones, D.K. (2004) The effect of gradient sampling schemes on measures derived from diffusion tensor MRI: a Monte Carlo study. *Magn. Reson. Med.*, **51**, 807-815.

Kawakami, Y., Abe, T. & Fukunaga, T. (1993) Muscle-fiber pennation angles are greater in hypertrophied than in normal muscles. *J. Appl. Physiol.* (*1985*), **74**, 2740-2744.

Kubo, K., Kawata, T., Ogawa, T., Watanabe, M. & Sasaki, K. (2006) Outer shape changes of human masseter with contraction by ultrasound morphometry. *Arch. Oral Biol.*, **51**, 146-153.

Lee, J.W., Kim, J.H., Kang, H.S., Lee, J.S., Choi, J.Y., Yeom, J.S., Kim, H.J. & Chung, H.W. (2006) Optimization of acquisition parameters of diffusion-tensor magnetic resonance imaging in the spinal cord. *Invest. Radiol.*, **41**, 553-559.

Li, X., Morgan, P.S., Ashburner, J., Smith, J. & Rorden, C. (2016) The first step for neuroimaging data analysis: DICOM to NIfTI conversion. *J. Neurosci. Methods*, **264**, 47-56.

Malik, B., Whittle, T., Ogawa, T. & Murray, G.M. (2018) Reorganization of motor unit activity at different sites within the human masseter muscle during experimental masseter pain. *Eur. J. Oral Sci.*, **126**, 400-410.

Mukherjee, P., Chung, S.W., Berman, J.I., Hess, C.P. & Henry, R.G. (2008) Diffusion tensor MR imaging and fiber tractography: technical considerations. *AJNR Am. J. Neuroradiol.*, **29**, 843-852.

Ng, H.P., Ong, S.H., Liu, J., Huang, S., Foong, K.W., Goh, P.S. & Nowinski, W.L. (2009) 3D segmentation and quantification of a masticatory muscle from MR data using patient-specific models and matching distributions. *J. Digit. Imaging*, **22**, 449-462.

Ogawa, T., Kawata, T., Tsuboi, A., Hattori, Y., Watanabe, M. & Sasaki, K. (2006) Functional properties and regional differences of human masseter motor units related to three-dimensional bite force. *J. Oral Rehabil.*, **33**, 729-740.

Ohrbach, R. (2014) Diagnostic criteria for temporomandibular disorders. Clinical protocol and assessment instruments. [Internet], [*Updated*: January 20, 2014], www.rdc-tmdinternational.org, International RDC/TMD Consortium Network.

Okada, C., Yamaguchi, S., Watanabe, Y., Watanabe, M. & Hattori, Y. (2016) Evaluation of masticatory activity during unilateral single tooth clenching using muscle functional magnetic resonance imaging. *J. Oral Rehabil.*, **43**, 583-590.

Oudeman, J., Nederveen, A.J., Strijkers, G.J., Maas, M., Luijten, P.R. & Froeling, M. (2016) Techniques and applications of skeletal muscle diffusion tensor imaging: a review. *J. Magn. Reson. Imaging*, **43**, 773-788.

Pereira, L.J., Gaviao, M.B., Bonjardim, L.R., Castelo, P.M. & van der Bilt, A. (2007) Muscle thickness, bite force, and craniofacial dimensions in adolescents with signs and symptoms of temporomandibular dysfunction. *Eur. J. Orthod.*, **29**, 72-78.

Saupe, N., White, L.M., Stainsby, J., Tomlinson, G. & Sussman, M.S. (2009) Diffusion tensor imaging and fiber tractography of skeletal muscle: optimization of B value for imaging at 1.5 T. *AJR Am. J. Roentgenol.*, **192**, W282-290.

Shiraishi, T., Chikui, T., Inadomi, D., Kagawa, T., Yoshiura, K. & Yuasa, K. (2012) Evaluation of diffusion parameters and T2 values of the masseter muscle during jaw opening, clenching, and rest. *Acta Radiol.*, **53**, 81-86.

Smith, S.M., Jenkinson, M., Woolrich, M.W., Beckmann, C.F., Behrens, T.E., Johansen-Berg, H., Bannister, P.R., De Luca, M., Drobnjak, I., Flitney, D.E., Niazy, R.K., Saunders, J., Vickers, J., Zhang, Y., De Stefano, N., et al. (2004) Advances in functional and structural MR image analysis and implementation as FSL. *Neuroimage*, **23** Suppl 1, S208-219.

Sotak, C.H. (2004) Nuclear magnetic resonance (NMR) measurement of the apparent diffusion coefficient (ADC) of tissue water and its relationship to cell volume changes in pathological states. *Neurochem. Int.*, **45**, 569-582.

Steidle, G. & Schick, F. (2006) Echoplanar diffusion tensor imaging of the lower leg musculature using eddy current nulled stimulated echo preparation. *Magn. Reson. Med.*, **55**, 541-548.

Stejskal, E.O. & Tanner, J.E. (1965) Spin diffusion measurements: spin echoes in the presence of a time-dependent field gradient. *J. Chem. Phys.*, **42**, 288-292.

Tonndorf, M.L., Sasaki, K. & Hannam, A.G. (1989) Single-wire recording of regional activity in the human masseter muscle. *Brain Res. Bull.*, **23**, 155-159.

Tournier, J.D, Calamante, F. & Connelly, A. (2010) Improved probabilistic streamlines tractography by 2nd order integration over fibre orientation distributions. Annual Meeting, 1-7 May 2010. *Intl. Soc. Mag. Reson. Med.*, Stockholm, Sweden.

Tournier, J.D., Smith, R., Raffelt, D., Tabbara, R., Dhollander, T., Pietsch, M., Christiaens, D., Jeurissen, B., Yeh, C.H. & Connelly, A. (2019) MRtrix3: a fast, flexible and open software framework for medical image processing and visualisation. *Neuroimage*, **202**, 116137.

van Dijk, J.P., Eiglsperger, U., Hellmann, D., Giannakopoulos, N.N., McGill, K.C., Schindler, H.J. & Lapatki, B.G. (2016) Motor unit activity within the depth of the masseter characterized by an adapted scanning EMG technique. *Clin. Neurophysiol.*, **127**, 3198-3204.

van Eijden, T.M. & Raadsheer, M.C. (1992) Heterogeneity of fiber and sarcomere length in the human masseter muscle. *Anat. Rec.*, **232**, 78-84.

Voskuilen, L., Mazzoli, V., Oudeman, J., Balm, A.J.M., van der Heijden, F., Froeling, M., de Win, M.M.L., Strijkers, G.J., Smeele, L.E. & Nederveen, A.J. (2019) Crossing muscle fibers of the human tongue resolved in vivo using constrained spherical deconvolution. *J. Magn. Reson. Imaging*, **50**, 96-105.

Yamamoto, A., Miki, Y., Urayama, S., Fushimi, Y., Okada, T., Hanakawa, T., Fukuyama, H. & Togashi, K. (2007) Diffusion tensor fiber tractography of the optic radiation: analysis with 6-, 12-, 40-, and 81-directional motion-probing gradients, a preliminary study. *AJNR Am. J. Neuroradiol.*, **28**, 92-96.